



Contents lists available at ScienceDirect

The International Journal of Biochemistry & Cell Biology

journal homepage: www.elsevier.com/locate/biocel

Review

New pyrrole-based histone deacetylase inhibitors: Binding mode, enzyme- and cell-based investigations

Antonello Mai^{a,*}, Sergio Valente^a, Angela Nebbioso^b, Silvia Simeoni^a, Rino Ragno^{a,**,1}, Silvio Massa^c, Gerald Brosch^d, Floriana De Bellis^{b,e}, Fabio Manzo^b, Lucia Altucci^{b,***,2}

^a Istituto Pasteur-Fondazione Cenci Bolognietti, Dipartimento di Studi Farmaceutici, Sapienza Università di Roma, P. le A. Moro 5, 00185 Roma, Italy

^b Dipartimento di Patologia Generale, Seconda Università degli Studi di Napoli, vico L. De Crecchio 7, 80138 Napoli, Italy

^c Dipartimento Farmaco Chimico Tecnologico, Università degli Studi di Siena, via A. Moro, 53100 Siena, Italy

^d Division of Molecular Biology, Biocenter, Innsbruck Medical University, Fritz-Preglstrasse 3, 6020 Innsbruck, Austria

^e Department of Cancer Biology, IGBCM, Strasbourg, France

ARTICLE INFO

Article history:

Available online 12 September 2008

Keywords:

Chromatin remodelling

Histone deacetylase

Aroyl-pyrrolyl-hydroxyamides

Apoptosis

Cytodifferentiation

ABSTRACT

Aroyl-pyrrolyl-hydroxy-amides (APHAs) are a class of synthetic HDAC inhibitors described by us since 2001. Through structure-based drug design, two isomers of the APHA lead compound **1**, the 3-(2-benzoyl-1-methyl-1H-pyrrol-4-yl)-N-hydroxy-2-propenamide **2** and the 3-(2-benzoyl-1-methyl-1H-pyrrol-5-yl)-N-hydroxy-2-propenamide **3** (iso-APHAs) were designed, synthesized and tested in murine leukemia cells as antiproliferative and cytodifferentiating agents. To improve their HDAC activity and selectivity, chemical modifications at the benzoyl moieties were investigated and evaluated using three maize histone deacetylases: HD2, HD1-B (class I human HDAC homologue), and HD1-A (class II human HDAC homologue). Docking experiments on HD1-A and HD1-B homology models revealed that the different compounds selectivity profiles could be addressed to different binding modes as observed for the reference compound SAHA. Smaller hydrophobic cap groups improved class II HDAC selectivity through the interaction with HD1-A Asn89-Ser90-Ile91, while bulkier aromatic substituents increased class I HDAC selectivity.

Taking into account the whole enzyme data and the functional test results, the described iso-APHAs showed a behaviour of class I/IIb HDACi, with **4b** and **4i** preferentially inhibiting class IIb and class I HDACs, respectively. When tested in the human leukaemia U937 cell line, **4i** showed altered cell cycle (S phase arrest), joined to high (51%) apoptosis induction and significant (21%) differentiation activity.

© 2008 Elsevier Ltd. All rights reserved.

1. Introduction

Histone deacetylases (HDACs) represent a family of enzymes that compete with histone acetyltransferases (HATs) to modulate chromatin structure and transcriptional activity *via* changes in the acetylation status of nucleosomal histones. Histones H2A, H2B, H3, and H4 exhibit acetyl groups at the ϵ -amino-terminal lysine residues within the tails extending from the histone octamer of the nucleosome core. Among them, histones H3 and H4 constitute the main targets of the HDAC enzymatic activity. Gene transcrip-

tion or repression is associated with the ability of transcriptionally competent genes to recruit either HAT or HDAC proteins to the promoters, respectively (Kouzarides, 1999; Cheung et al., 2000; Strahl and Allis, 2000; Wolffe and Guschin, 2000; Wu and Grunstein, 2000).

Aberrant regulation of this epigenetic mechanism has been clearly linked to carcinogenesis, and a growing number of cancer diseases are reported to be associated with an alteration of the HAT/HDAC balance. In particular, it has been widely established that inappropriate HDAC-mediated transcriptional repression represents a common molecular mechanism used by oncoproteins to produce both alterations in the chromatin structure and blockage of normal cell differentiation. In this scenario, HDAC inhibitors (HDACi) can remove the epigenetic block of gene transcription, thus allowing cells to re-start differentiation gene programs or proapoptotic events (Bolden et al., 2006; Minucci and Pelicci, 2006). In addition to the modulation of gene expression through nucleosome remodeling, HDACi can regulate the acetylation status of a series

* Corresponding author. Tel.: +39 06 4991 3392; fax: +39 06 491491.

** Corresponding author. Tel.: +39 06 4991 3937; fax: +39 06 491491.

*** Corresponding author. Tel.: +39 081 566 7569; fax: +39 081 450 169.

E-mail addresses: antonello.mai@uniroma1.it (A. Mai), rino.ragno@uniroma1.it (R. Ragno), lucia.altucci@unina2.it (L. Altucci).

¹ Molecular modelling.

² Biology.

of non-histone targets, such as transcription factors (i.e., p53, YY1, STAT3, c-MYC, MyoD, E2F/Rb, and others) or other cellular proteins (i.e., α -tubulin, Ku70, HSP90, and others) (Glozak et al., 2005). Note that the dynamic acetylation of these targets has pleiotropic effects on many cellular functions, being often associated to anticancer activities (Budillon et al., 2007; Condorelli et al., 2008).

To date, eighteen mammalian HDACs have been identified and classified into four classes according to their homology to yeast deacetylases. Class I/II/IV HDACs are zinc ion dependent deacetylases, and are mainly localized in the nucleus (class I/IV) or shuttling between nucleus and cytoplasm (class II). Class I HDACs are ubiquitous whereas class II/IV HDACs display tissue-specific expression. Class III HDACs (sirtuins, SIRT1–7) share no sequence similarity with class I/II/IV HDACs, require NAD⁺ as a cofactor for their catalysis, and are mainly insensitive to class I/II/IV HDACi (Grozinger and Schreiber, 2002).

To date, a wide range of structures have been identified as inhibitors of class I/II/IV HDACs, but only a small number of molecules shows selectivity for a particular class/isoform of HDACs (Butler and Kozikowski, 2008; Itoh et al., 2008; Jones and Steinkuhler, 2008; Khan et al., 2008).

In October 2006, suberoylanilide hydroxamic acid (SAHA, vorinostat, Zolinza), a well-known HDACi, has been approved by FDA for the treatment of the advanced primary cutaneous T-cell lymphoma (CTCL) (Grant et al., 2007; Marks and Breslow, 2007). Vorinostat and other HDACi are currently in phase I/II or phase II/III clinical trials, alone or in combination with other drugs, for the treatment of a wide range of solid and haematological tumors. Nevertheless, in some cases their potential for clinical drug development has been limited by cytotoxicity (CHAPs, LAQ-824), low potency and lack of selectivity (sodium butyrate, sodium valproate), low solubility in the aqueous vehicle and/or low stability in cell culture and/or in *in vivo* assays [trichostatin A (TSA) and other hydroxamates] (Vigushin and Coombes, 2002). Thus, the development of more potent and/or selective HDACi represents a very attractive goal to pursue for the development of anticancer therapies. Selective compounds could be very useful tools to distinguish the different functions of the HDAC enzymes, and might represent highly specific anticancer therapeutic drugs with reduced toxicity.

In 2001, we have described a new class of HDAC inhibitors, named aroyl-pyrrolyl-hydroxy-amides (APHAs), with compound **1** being the lead molecule (Fig. 1) (Massa et al., 2001; Mai et al., 2002, 2003, 2004, 2006, 2007; Ragno et al., 2006, 2008). By structure-based drug design and docking procedures, the 3-(2-benzoyl-1-methyl-1H-pyrrol-4-yl)-N-hydroxy-2-propenamide **2** and the 3-(2-benzoyl-1-methyl-1H-pyrrol-5-yl)-N-hydroxy-2-propenamide **3**, two APHA isomers called *iso*-APHAs, have been discovered as novel leads (Fig. 1) (Ragno et al., 2004). Both **2** and **3** showed inhibitory activity against both maize HD2 and mouse HDAC1, with **2** being more active than **1** and **3** and as potent as SAHA, used as reference drug. Furthermore, cellular studies proved **2** to be an efficient antiproliferative and cytodifferentiating agent in the Friend murine erythroleukemia cell line (Ragno et al., 2004). Here, we report on the effect of chemical modifications applied to the benzoyl moieties of **2** and **3** on the HDAC inhibitory activity. The newly synthesized derivatives (compounds **4** and **5**, Fig. 1) were routinely tested against maize HD2 (Lusser et al., 1997), a plant specific deacetylase, and against maize HD1-B and HD1-A enzymes (Brosch et al., 1996a; Kollé et al., 1999; Lechner et al., 2000), two class I and class II HDAC homologues, respectively. Furthermore, their binding modes in the virtual HD1-B and HD1-A structures were investigated. Selected *iso*-APHAs were then tested against human HDAC1 and HDAC4 immunoprecipitates (IPs), and into functional assays such as histone H3 and α -tubulin acetylation potential in the human leukemia U937 cell line. Finally, the effects

of selected *iso*-APHAs on cell cycle, apoptosis induction, and granulocytic differentiation in the U937 cell line have been determined.

2. Materials and methods

2.1. Chemistry

For the synthesis of the title compounds, the key intermediates 2-aroyl-1-methyl-1H-pyrrol-4-yl and -5-yl carboxaldehydes **7a–i** and **8a–i** were prepared through a two-step Friedel–Craft/Vilsmeier–Haack procedure, starting from 1-methyl-1H-pyrrole and the proper aroyl chloride in the presence of boron trifluoride diethyl etherate, and further reaction of the obtained 2-aroyl-1-methyl-1H-pyrroles **6a–i** with oxalyl chloride and *N,N*-dimethylformamide. The pyrrolecarboxaldehydes **7** and **8** were treated with triethyl phosphonoacetate in the presence of potassium carbonate under Wittig–Horner conditions to afford the related ethyl pyrrole-4-propenoates and -5-propenoates (**9a–i** and **10a–i**), which were in turn converted into the corresponding pyrrolepropenoic acids (**11a–i** and **12a–i**) by alkaline hydrolysis. Finally, the reaction of **11** and **12** with ethyl chloroformate and *O*-(2-methoxy-2-propyl)hydroxylamine followed by removal of the *O*-protection with Amberlyst 15 ion-exchange resin furnished the desired hydroxamates **4a–i** and **5a–i** (Scheme 1). Chemical and physical data for compounds **4a, b, d–i** and **5a–i** are listed in Table 1. Chemical and physical data for the unknown intermediate compounds **6b, g, i, 7a, b, d, e, g–i, 8a, b, d–i, 9a, b, d–i, 10a, b, d–i, 11a–i, and 12a–h** are listed in Table 2. The 2-aroyl-1-methyl-1H-pyrroles **6a** (R=2-Me-Ph) (Marumo et al., 2002), **6c** (R=4-Me-Ph) (Artico et al., 1982), **6d–f** (R=2-, 3-, and 4-Cl-Ph, respectively) (Carson and Davis, 1981; Carson et al., 2000), and **6h** (R=2-naphthyl) (Carson and Pitis, 2002) were already described. The pyrrolealdehydes **7c** (R=4-Me-Ph) (Artico et al., 1982), **7f** (R=4-Cl-Ph) (Carson et al., 2003a,b), and **8c** (R=4-Me-Ph) (Artico et al., 1982), the ethyl esters **9c** and **10c** (R=4-Me-Ph for both) (Corelli et al., 1987), the pyrroleacrylic acid **12i** (R=4-biphenyl) (Lee et al., 1996), and the hydroxamate **4c** (R=4-Me-Ph) (Corelli et al., 1987) were also previously reported.

2.2. Synthesis of compounds

Melting points were determined on a Büchi 530 melting point apparatus and are uncorrected. Infrared (IR) spectra (KBr) were recorded on a PerkinElmer Spectrum One instrument. ¹H NMR spectra were recorded at 200 MHz on a Bruker AC 200 spectrometer; chemical shifts are reported in δ (ppm) units relative to the internal reference tetramethylsilane (Me₄Si). All compounds were routinely checked by TLC and ¹H NMR. TLC was performed on aluminum-backed silica gel plates (Merck DC-Alufolien Kieselgel 60 F₂₅₄) with spots visualized by UV light. All solvents were reagent grade and, when necessary, were purified and dried by standard methods. Concentration of solutions after reactions and extractions involved the use of a rotary evaporator operating at a reduced pressure of \approx 20 Torr. Organic solutions were dried over anhydrous sodium sulfate. Analytical results are within \pm 0.40% of the theoretical values. A SAHA sample for biological assays was prepared as previously reported by us. All chemicals were purchased from Aldrich Chimica, Milan (Italy) or Lancaster Synthesis GmbH, Milan (Italy) and were of the highest purity.

General procedure for the synthesis of 2-aroyl-1-methyl-1H-pyrroles (**6b, g, i**). Example: 2-(4-phenylbenzoyl)-1-methyl-1H-pyrrole (**6i**). 1-Methyl-1H-pyrrole (24.65 mmol; 2.2 ml) was added to a solution of 4-biphenylcarbonyl chloride (49.3 mmol; 10.68 g) and boron trifluoride diethyl etherate (49.3 mmol; 6.19 ml) in

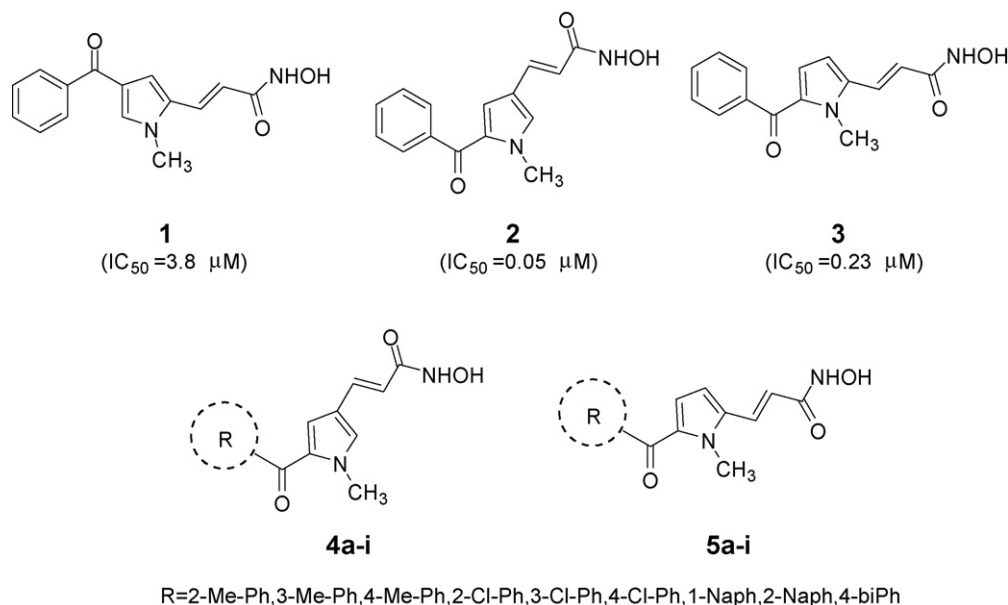
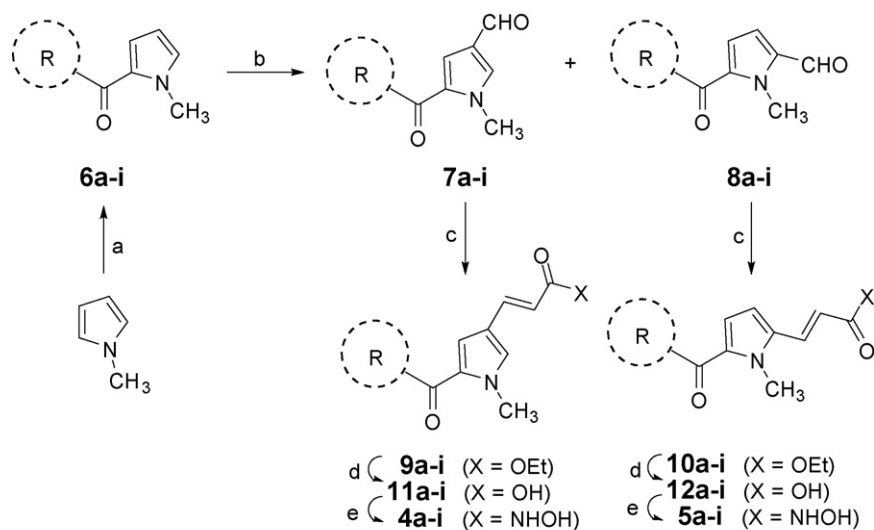


Fig. 1. The APHA lead compound **1**, its isomers **2** and **3** and the novel *iso*-APHAs **4a-i** and **5a-i**. For **1–3** the IC_{50} values against maize HD2 have been reported.

dichloromethane (100 ml). After being stirred at room temperature for 3 days, water (100 ml) was slowly added to the reaction mixture. The organic layer was separated, and the aqueous phase was extracted with chloroform (3×50 ml). The combined organic solutions were washed with water, dried, and evaporated to dryness. The residual oil was chromatographed on silica gel eluting with ethyl acetate:*n*-hexane 1:10 to give the pure compound **6i**. 1H NMR ($CDCl_3$) δ 4.06 (s, 3H, N- CH_3), 6.18 (m, 1H, pyrrole β -proton), 6.81 (m, 1H, pyrrole β -proton), 6.94 (m, 1H, pyrrole α -proton), 7.40–7.50 (m, 3H, biphenyl H-3'-5'), 7.64–7.69 (m, 4H, biphenyl H-3,5,2',6'), 7.90 (d, 2H, biphenyl H-2,6).

General procedure for the synthesis of 5-*aroyl*-1-methyl-1*H*-pyrrole-3-carboxaldehydes (**7a, b, d, e, g-i**) and -2-carboxaldehydes (**8a, b, d-i**). Example: 5-(3-chlorobenzoyl)-

1-methyl-1*H*-pyrrole-2-carboxaldehyde (**7e**) and 5-(3-chlorobenzoyl)-1-methyl-1*H*-pyrrole-3-carboxaldehyde (**8e**). A solution of oxalyl chloride (60 mmol, 5.2 ml) in 1,2-dichloroethane (50 ml) was added to a cooled ($0-5^\circ C$) solution of dry *N,N*-dimethylformamide (60 mmol, 4.6 ml) in 1,2-dichloroethane (50 ml), over a period of 5–10 min. After 15 min, a solution of 2-(3-chlorobenzoyl)-1-methyl-1*H*-pyrrole (**6e**) (60 mmol, 13.2 g) in 1,2-dichloroethane (50 ml) was slowly added to the suspension. The mixture was stirred at room temperature for 1 h, then was poured onto crushed ice (200 g) containing 50% NaOH (50 ml) and stirred for 10 min. Afterwards, the aqueous solution was extracted with chloroform (3×50 ml), and the combined organic extracts were washed with water (100 ml), dried, and evaporated to dryness. The residual oil was chromatographed on silica gel



R = 2-Me-Ph (a), 3-Me-Ph (b), 4-Me-Ph (c), 2-Cl-Ph (d), 3-Cl-Ph (e), 4-Cl-Ph (f), 1-naphthyl (g), 2-naphthyl (h), 4-biphenyl (i)

Scheme 1. Synthesis of compounds **4a-i** and **5a-i**. Reagents: (a) $BF_3 \cdot Et_2O$, $RCOCl$, CH_2Cl_2 ; (b) – (1) DMF, $(COCl)_2$, $(CH_2)_2Cl_2$; (2) 50% NaOH; (c) $(EtO)_2POCH_2COOEt$, anhydrous K_2CO_3 , EtOH; (d) 2N KOH, EtOH; (e) – (1) $ClCOOEt$, Et_3N , anhydrous THF; (2) $CH_3OC(CH_3)_2ONH_2$, anhydrous THF; (3) amberlyst 15, MeOH.

Table 1
Chemical and physical data of compounds **4a**, **b**, **d–i** and **5a–i**^a.

Compound	R	Melting point (°C)	Crystallization solvent	Yield (%)
4a	2-Me-Ph	218–220	Benzene/acetonitrile	98
4b	3-Me-Ph	168–169	Benzene/acetonitrile	98
4d	2-Cl-Ph	146–148	Benzene	95
4e	3-Cl-Ph	164–165	Benzene/acetonitrile	89
4f	4-Cl-Ph	165–166	Benzene/acetonitrile	89
4g	1-Naphthyl	140–141	Benzene	88
4h	2-Naphthyl	205–206	Benzene/acetonitrile	79
4i	4-Biphenyl	184–186	Acetonitrile	98
5a	2-Me-Ph	114–115	Benzene	77
5b	3-Me-Ph	125–126	Benzene/acetonitrile	66
5c	4-Me-Ph	151–152	Benzene/acetonitrile	90
5d	2-Cl-Ph	Oil		78
5e	3-Cl-Ph	100–101	Acetonitrile	85
5f	4-Cl-Ph	132–133	Acetonitrile	98
5g	1-Naphthyl	Oil		98
5h	2-Naphthyl	126–127	Benzene/acetonitrile	78
5i	4-Biphenyl	150–151	Acetonitrile	93

^a Analytic results were within $\pm 0.40\%$ of the theoretical values.

eluting with ethyl acetate:chloroform 1:10. The first eluates were collected and evaporated to afford **8e** as a pure solid; further elution gave **7e** as a pure solid. **7e**: ¹H NMR (CDCl₃) δ 4.07 (s, 3H, N-CH₃), 7.15 (s, 1H, pyrrole β -proton), 7.42 (t, 1H, benzene H-5), 7.55 (m, 2 H, benzene H-4,6), 7.67 (m, 1H, benzene H-2), 7.78 (s, 1H, pyrrole α -proton), 9.79 (s, 1H, CHO). **8e**: ¹H NMR (CDCl₃) δ 4.28 (s, 3H, N-CH₃), 6.67 (d, 1H, pyrrole β -proton), 6.92 (d, 1H, pyrrole β -proton), 7.26–7.81 (m, 4H, benzene H-2,4-6), 9.83 (s, 1H, CHO).

General procedure for the synthesis of ethyl 3-[(5-*aroyl*)-1-methyl-1*H*-3-pyrrolyl]-2-propenoates (**9a**, **b**, **d–i**) and 3-[(5-*aroyl*)-1*H*-1-methyl-2-pyrrolyl]-2-propenoates (**10a**, **b**, **d–i**). Example: ethyl 3-[5-(2-naphthoyl)-1-methyl-1*H*-3-pyrrolyl]-2-propenoate (9h). A suspension of 7h (1.03 mmol, 0.27 g) in dry ethanol (20 ml) was added in one portion to a mixture of triethyl phosphonoacetate (1.24 mmol, 0.25 ml) and anhydrous potassium carbonate (2.06 mmol, 0.28 g). After stirring at 70 °C for 2 h, the reaction mixture was cooled to room temperature, eluted with water (50 ml) and extracted with ethyl acetate (3 \times 30 ml). The organic layer was washed with water, dried with sodium sulphate and evaporated to dryness, the solid residue was recrystallized by cyclohexane to furnish pure **9h**. ¹H NMR (CDCl₃) δ 1.28 (m, 3H, CH₂CH₃), δ 4.06 (s, 3H, N-CH₃), 4.21 (m, 3H, CH₂CH₃), 6.10 (d, 1H, CH = CHCOOEt), 6.96 (d, 1H, pyrrole β -proton), 7.15 (s, 1H, pyrrole α -proton), 7.53–7.61 (m, 3H, CH = CHCOOEt, naphthalene H-6,7), 7.87–7.97 (m, 4H, naphthalene H-3,4,5,8), 8.32 (s, 1H, naphthalene H-1).

General procedure for the synthesis of 3-[(5-*aroyl*)-1-methyl-1*H*-3-pyrrolyl]-2-propenoic acids (**11a–i**) and 3-[(5-*aroyl*)-1-methyl-1*H*-2-pyrrolyl]-2-propenoic acids (**12a–h**). Example: 3-[5-(3-methylbenzoyl)-1-methyl-1*H*-2-pyrrolyl]-2-propenoic acid (**12b**). A mixture of **10b** (3.13 mmol, 0.93 g), 2 N KOH (12.52 mmol, 0.70 g) and ethanol (15 ml) was stirred at room temperature overnight. Afterwards, the solution was poured into water (50 ml) and extracted with ethyl acetate (3 \times 20 ml). Then, 2 N HCl solution (50 ml) was added to the aqueous layer, and the precipitate was filtered and recrystallized by acetonitrile to give the pure compound **12b**. ¹H NMR (DMSO-*d*₆) δ 2.42 (s, 3H, 3-CH₃), 4.08 (s, 3H, N-CH₃), 6.40 (d, 1H, CH = CHCOOH), 6.70 (m, 2H, pyrrole β -protons), 7.35 (m, 2H, benzene H-3,4), 7.60 (m, 2H, benzene H-2,6), 7.79 (d, 1H, CH = CHCOOH), 12.0 (s, 1H, COOH).

General procedure for the synthesis of 3-[(5-*aroyl*)-1-methyl-1*H*-3-pyrrolyl]-*N*-hydroxy-2-propenamides (**4a**, **b**, **d–i**) and 3-[(5-*aroyl*)-1-methyl-1*H*-2-pyrrolyl]-*N*-hydroxy-2-propenamides (**5a–i**). Example: 3-[5-(4-phenylbenzoyl)-1-methyl-1*H*-3-pyrrolyl]-*N*-hydroxy-2-propenamide (**4i**). Ethyl chloroformate

(1.88 mmol, 0.18 ml) and triethylamine (2.04 mmol, 0.28 ml) were added to a cooled (0 °C) solution of **11i** (1.57 mmol, 0.50 g) in dry tetrahydrofuran (10 ml), and the mixture was stirred for 10 min. The solid was filtered off and *O*-(2-methoxypropyl)-hydroxylamine (4.71 mmol, 0.35 ml) was added to the filtrate. The solution was stirred for 15 min at 0 °C, then the mixture was evaporated under reduced pressure, the residue was diluted in methanol (10 ml), and Amberlyst 15 (157 mg) was added to the solution of the protected hydroxamate. The mixture was stirred for 1 h, then the resin was filtered and the filtrate was concentrated in vacuo to give **4i**, which was recrystallized from acetonitrile. ¹H NMR (DMSO-*d*₆) δ 3.94 (s, 3H, N-CH₃), 6.10 (d, 1H, CH = CHCONHOH), 6.89 (s, 1H, pyrrole β -proton), 7.28 (d, 1H, CH = CHCONHOH), 7.43 (t, 1H, biphenyl H-4'), 7.49 (d, 2H, biphenyl H-3,5), 7.59 (s, 1H, pyrrole α -proton), 7.74 (d, 2H, biphenyl H-2,6), 7.84 (s, 4H, biphenyl H-2',3',5',6'), 8.85 (s, 1H, NHOH), 10.48 (s, 1H, NHOH).

2.3. *In vitro* maize HD1-B, HD1-A, and HD2 enzyme inhibition

Radioactively labeled chicken core histones were used as the enzyme substrate according to established procedures (Brosch et al., 1996a,b; Lechner et al., 1996; Kollé et al., 1998). The enzymatic activity liberated tritiated acetic acid from the substrate, which was quantified by scintillation counting. IC₅₀ values are results of triple determinations. A 50 μ l sample of maize enzyme was incubated (30 min, 30 °C) with 10 μ l of total [³H]acetate-prelabeled chicken reticulocyte histones (2 mg/ml). Reaction was stopped by addition of 36 μ l of 1 M HCl/0.4 M acetate and 800 μ l of ethyl acetate. After centrifugation (10,000 \times g, 5 min), an aliquot of 600 μ l of the upper phase was counted for radioactivity in 3 ml of liquid scintillation cocktail. The compounds were tested at a starting concentration of 40 μ M, and active substances were diluted further. TSA and SAHA were used as the reference compounds, and blank solvents were used as negative controls.

2.4. Homology models, molecular modelling and docking studies

All molecular modelling software run on IBM compatible AMD Athlon 3.0 Ghz workstations with the Linux operating system SUSE 9.0 distribution.

2.4.1. HD1-A and HD1-B 3D models preparation

The class I (HD1-B) and class II (HD1-A) HDAC homologues structures were prepared using the respective sequence deposited

Table 2Chemical and physical data of compounds **6b**, **g**, **i**, **7a**, **b**, **d**, **e**, **g**–**i**, **8a**, **b**, **d**–**i**, **9a**, **b**, **d**–**i**, **10a**, **b**, **d**–**i**, **11a**–**i**, and **12a**–**h**^a.

Compound	R	Melting point (°C)	Crystallization solvent	Yield (%)
6b	3-Me-Ph	Oil		69
6g	1-Naphthyl	116–118	Cyclohexane	64
6i	4-Biphenyl	81–83	Cyclohexane	63
7a	2-Me-Ph	Oil		22
7b	3-Me-Ph	Oil		36
7d	2-Cl-Ph	123–125	Cyclohexane	24
7e	3-Cl-Ph	115–116	Cyclohexane/benzene	32
7g	1-Naphthyl	Oil		21
7h	2-Naphthyl	145–146	Cyclohexane	25
7i	4-Biphenyl	148–149	Cyclohexane/benzene	40
8a	2-Me-Ph	114–115	Cyclohexane/benzene	26
8b	3-Me-Ph	125–126	Cyclohexane	29
8d	2-Cl-Ph	Oil		23
8e	3-Cl-Ph	100–101	Cyclohexane	35
8f	4-Cl-Ph	132–133	Cyclohexane/benzene	28
8g	1-Naphthyl	Oil		23
8h	2-Naphthyl	126–127	Cyclohexane/benzene	27
8i	4-Biphenyl	150–151	Cyclohexane/benzene	43
9a	2-Me-Ph	Oil		76
9b	3-Me-Ph	109–110	Cyclohexane/benzene	89
9d	2-Cl-Ph	143–145	Cyclohexane/benzene	95
9e	3-Cl-Ph	155–156	Benzene	84
9f	4-Cl-Ph	135	Benzene	87
9g	1-Naphthyl	Oil		93
9h	2-Naphthyl	100–101	Cyclohexane	91
9i	4-Biphenyl	146–147	Cyclohexane/benzene	87
10a	2-Me-Ph	Oil		69
10b	3-Me-Ph	112–113	Cyclohexane	85
10d	2-Cl-Ph	163–164	Cyclohexane/benzene	93
10e	3-Cl-Ph	158–159	Benzene	90
10f	4-Cl-Ph	127–128	Benzene	87
10g	1-Naphthyl	Oil		89
10h	2-Naphthyl	110–111	Cyclohexane	94
10i	4-Biphenyl	157–158	Cyclohexane/benzene	78
11a	2-Me-Ph	201–202	Benzene/acetonitrile	79
11b	3-Me-Ph	159–160	Acetonitrile	99
11c	4-Me-Ph	159–160	Acetonitrile	98
11d	2-Cl-Ph	193–195	Benzene/acetonitrile	97
11e	3-Cl-Ph	185–186	Acetonitrile	86
11f	4-Cl-Ph	228–229	Acetonitrile	92
11g	1-Naphthyl	206–207	Acetonitrile	79
11h	2-Naphthyl	231–232	Benzene/acetonitrile	85
11i	4-Biphenyl	242–243	Benzene/acetonitrile	79
12a	2-Me-Ph	188–189	Acetonitrile	77
12b	3-Me-Ph	162–163	Acetonitrile	98
12c	4-Me-Ph	180–181	Acetonitrile	89
12d	2-Cl-Ph	158–160	Acetonitrile	95
12e	3-Cl-Ph	180–181	Acetonitrile	89
12f	4-Cl-Ph	201–202	Acetonitrile	90
12g	1-Naphthyl	199–200	Benzene	81
12h	2-Naphthyl	237–238	Benzene/acetonitrile	88

^a Analytic results were within $\pm 0.40\%$ of the theoretical values.

in the TrEMBL Protein Database (entry codes P56521 for HD1-B and Q7XAX9 for HD1-A). The homology models were automatically obtained by feeding the CPHmodels 2.0 Server with the above sequences and using the HDAC8/TSA complex as template (pdb entry code 1t64) (Somoza et al., 2004). The two models were then refined by the AMBER 8.0 program (Case et al., 2005) using the following protocol. First, the experimental bound conformation of TSA as found in the template was merged into either HD1-A or HD1-B structures. AM1-BCC charges were calculated on the TSA employing the antechamber module of Amber 8.0. Using the xLeap AMBER module, the starting complexes were added of the hydrogen atoms and solvated in a octahedral box of Monte Carlo TIP3P water with each box side at least 10.0 Å away from the nearest atoms of the complexes. Sodium ions were included to neutralize the charge of the system. The ions were placed randomly (by replacing water molecules) in the system 10 Å away from each other and from the nearest atoms. The hydrogen atoms, counter

ions, and water molecules were then minimized for 1000 iterations. Then the whole complexes were relaxed for 5000 iterations. The MD simulations were performed with the smooth Particle-mesh Ewald (PME) method employed to accommodate long-range electrostatic forces and with periodic boundary conditions at constant volume. The simulations utilized the Amber all-atom (parm99) and the GAFF force fields with a step size of 2 femtoseconds (fs). By using an extended list technique, the non-bonded interactions were effectively updated every step with a small overhead in computational cost. The non-bonded cut-off for van der Waals interactions was set to 10 Å. All covalent bonds involving hydrogen atoms were constrained using SHAKE. The ions and water molecules were then equilibrated for 20 ps at constant volume followed by energy minimization while freezing the model complex. Then a second equilibration was carried out for 90 ps while gradually unfreezing the bound TSA. A final equilibration of further 150 ps was carried out on the whole complexes without any restrain. During the equilibra-

tions the stability of the complexes were monitored via their root mean square deviations (RMSD). By the mean of the ptraj module the average structures were obtained from the last part of equilibrations and energy minimized for 1000 iterations. Deletions of the bound TSA molecules lead to the HD1-A and HD1-B models used for the subsequent docking studies.

2.4.2. Docking procedure

The docking studies were performed using AutoDock 3.0.5 and AutoDock 4.0.1 (Goodsell et al., 1996; Morris et al., 1996, 1998). The proteins [HD1-A, HD1-B, HDAH (1ZZ1) and HDLP (1C3S) (Finnin et al., 1999; Nielsen et al., 2005)] were aligned by means of UCSF Chimera MatchMaker tool (Pettersen et al., 2004). The molecular structures of derivatives **4** and **5** were drawn using a in house protocol employing the jchempaint (<http://jchempaint.sourceforge.net/>) software (Krause et al., 2000), converted into three-dimensional structure using the CDK libraries (Steinbeck et al., 2003, 2006) implemented in our web server (<http://rcmd-server.frm.uniroma1.it/rcmd-portal>) which afforded directly the molecules ready to be used in the molecular docking software. Prior docking, the compounds were aligned to HD1-A and HD1-B SAHA conformations using Surfex software (Jain, 2007). We noted that this preventive alignment led to more consistent docking simulations with fewer and more populated clusters (data not shown). AutoDock Tools package 1.4.4 was employed to generate the docking input files and to analyze the docking results; the same procedure as described in the manual was followed. The proteins were consider rigid except HD1-A/Tyr306, HD1-B/Tyr298, 1ZZ1/Tyr311 and 1C3S/Tyr296. A grid box size of 60 × 60 × 70 points with a spacing of 0.375 Å between the grid points was implemented and centered to the bound SAHA covered most of the catalytic channel of either enzymes. For all the inhibitors, the single bonds excluding the amide bonds were treated as active torsional bonds. One hundred structures, i.e. 100 runs, were generated by using genetic algorithm searches. A default protocol was applied, with an initial population of 150 randomly placed individuals, a maximum number of 2.5×10^6 energy evaluations, and a maximum number of 2.7×10^4 generations. A mutation rate of 0.02 and a crossover rate of 0.8 were used. In parallel docking experiments the bound SAHA molecules extracted from either average MD equilibrated complexes were docked back into the HD1-A and HD1-B enzymes. AutoDock proved to reposition the SAHA with an acceptable root mean square deviation (RMSD) error ($\text{RMSD}_{\text{SAHA-HD1-A}} = 1.42$, $\text{RMSD}_{\text{SAHA-HD1-B}} = 2.21$).

The whole re-docking procedure was also applied to the experimental class I [HDLP (Finnin et al., 1999)] and class II [HDAH (Nielsen et al., 2005)] HDACs complexed with SAHA affording to low RMSD values ($\text{RMSD}_{\text{SAHA/HDLP}} = 1.28$, $\text{RMSD}_{\text{SAHA/HDAH}} = 1.58$) and furthermore assessing the use of the AutoDock program.

2.5. Cellular assays

2.5.1. Cell lines and cultures

U937 cell line was cultured in RPMI with 10% fetal calf serum, 100 U/ml penicillin, 100 µg/ml streptomycin and 250 ng/ml amphotericin-B, 10 mM HEPES and 2 mM glutamine. U937 cells were kept at the constant concentration of 200,000 cells per ml of culture medium. Human breast cancer ZR-75.1 cells were propagated in DMEM medium supplemented with 10% fetal calf serum and antibiotics (100 U/ml penicillin, 100 µg/ml streptomycin and 250 ng/ml amphotericin-B).

2.5.2. Cell-based human HDAC1 and HDAC4 assays

Cells (U937 cells for the HDAC1 assay; ZR75.1 cells for the HDAC4 assay) were lysed in IP buffer (Tris-HCl pH 7.0, 50 mM, NaCl,

180 mM, NP-40, 0.15%, glycerol, 10%, MgCl₂, 1.5 mM, NaMO₄ 1 mM, NaF 0.5 mM) with protease inhibitor cocktail (Sigma), DTT 1 mM and PMSF 0.2 mM for 10 min in ice and centrifugated at 13,000 rpm for 30 min. 1000 µg of extracts were diluted in IP buffer up to 1 ml and pre-cleared by incubating with 20 µl A/G plus Agarose (Santa Cruz) for 1 h on a rocking table at 4 °C. Supernatants were transferred into a new tube and the antibodies (around 3 µg) were added and IP was allowed to proceed overnight at 4 °C on a rocking table. Antibodies used: HDAC1 (Abcam) and HDAC4 (Sigma). As negative control the same amount of protein extracts were immunoprecipitated with the corresponding purified IgG (Santa Cruz). The day after 20 µl A/G plus Agarose (Santa Cruz) were added to each IP and incubation was continued for 2 h. The beads were recovered by brief centrifugation and washed with cold IP buffer several times. The samples were than washed twice in PBS and re-suspended in 20 µl of sterile PBS. The HDAC assay was carried out according to suppliers instructions (Upstate). Briefly, samples immunoprecipitated with HDAC4 and HDAC1 or with purified IgG were pooled respectively to homogenize all samples. 10 µl of the IP was incubated with a previously labelled ³H-histone H4 peptide linked with streptavidine agarose beads (Upstate). In details, 120,000 cpm of the H₄-³H-acetyl-peptide was used for each tube and incubated in 1 × HDAC buffer with 10 µl of the sample in presence or absence of HDAC inhibitors with a final volume of 200 µl. Those samples were incubated over night at 37 °C in slow rotation. The day after 50 µl of a quenching solution were added and 100 µl of the samples were counted in duplicate after a brief centrifugation in a scintillation counter. Experiments have been carried out in quadruplicate.

2.5.3. Cell cycle analysis on U937 cells

2.5×10^5 cells were collected and resuspended in 500 µl of an hypotonic buffer (0.1% Triton X-100, 0.1% sodium citrate, 50 µg/ml propidium iodide (PI), and RNase A freshly added). Cells were incubated in the dark for 30 min. Samples were acquired on a FACS-Calibur flow cytometer using the Cell Quest software (Becton Dickinson) and analysed with standard procedures using the Cell Quest software (Becton Dickinson) and the ModFit LT version 3 Software (Verity) as previously reported (Nebbio et al., 2005). All the experiments were performed three times.

2.5.4. FACS analysis of apoptosis on U937 cells

Apoptosis was measured with Annexin V/PI double staining detection (Roche and Sigma-Aldrich, respectively) as recommended by the suppliers; samples were analysed by FACS with Cell Quest technology (Becton Dickinson) as previously reported (Altucci et al., 2001). As second assays the caspase 3 detection (B-Bridge) was performed and quantified by FACS (data not shown; Becton Dickinson).

2.5.5. Caspase 8 and 9 activity on U937 cells

Caspase 8 and 9 activity assays were performed as recommended by the suppliers (B-Bridge) in the U937 cells treated with compound **4i** at 5 µM for 18 h. SAHA at 5 µM was used as reference compound. TNF-related apoptosis-inducing ligand (TRAIL) and DR5 induction on U937 cells

2.5.6.1. RT-PCRs, PCR and primers. Total RNA has been extracted (Gibco) from the U937 cells treated for 6 h as indicated (both **4i** and SAHA at 5 µM). 2 µg was reverse transcribed using oligo dT primer and Superscript reverse transcriptase (Invitrogen). For amplification we have used the following primers:

Trail	Forward: 5'-caa ctc cgt cag ctc gtt aga aag Reverse: 5'-tta gac caa caa cta ttt cta cga ct
DR5	Forward: 5'-gcc tca tgg aca atg aga taa agg tgg ct Reverse: 5'-cca aat ctc aaa gta cgc aca aac gg

Table 3
Maize HD2, HD1-B, and HD1-A inhibitory activity of compounds **4a–i** and **5a–i**^a

Compound	R	IC ₅₀ (μM)			Selectivity	
		HD2	HD1-B	HD1-A	Class I	Class II
4a	2-Me-Ph	0.06 ± 0.002	0.13 ± 0.005	0.01 ± 0.0005		13
4b	3-Me-Ph	0.10 ± 0.005	0.17 ± 0.008	0.02 ± 0.001		9
4c	4-Me-Ph	0.15 ± 0.006	0.07 ± 0.003	0.17 ± 0.007		
4d	2-Cl-Ph	0.20 ± 0.012	0.32 ± 0.010	0.12 ± 0.006		
4e	3-Cl-Ph	0.18 ± 0.011	0.24 ± 0.007	0.05 ± 0.003		5
4f	4-Cl-Ph	0.16 ± 0.005	0.17 ± 0.005	0.07 ± 0.003		
4g	1-Naphthyl	0.01 ± 0.0005	0.01 ± 0.0003	0.07 ± 0.003	7	
4h	2-Naphthyl	0.05 ± 0.002	0.09 ± 0.004	0.04 ± 0.002		
4i	4-Biphenyl	0.05 ± 0.002	0.03 ± 0.001	0.15 ± 0.007	5	
5a	2-Me-Ph	0.31 ± 0.015	0.41 ± 0.016	0.31 ± 0.012		
5b	3-Me-Ph	0.19 ± 0.004	0.22 ± 0.007	0.10 ± 0.003		
5c	4-Me-Ph	0.19 ± 0.006	0.39 ± 0.012	0.09 ± 0.004		4
5d	2-Cl-Ph	0.32 ± 0.013	1.59 ± 0.079	0.68 ± 0.020		
5e	3-Cl-Ph	0.09 ± 0.003	1.04 ± 0.052	0.10 ± 0.003		10
5f	4-Cl-Ph	0.24 ± 0.014	0.44 ± 0.022	0.13 ± 0.003		
5g	1-Naphthyl	0.13 ± 0.004	0.05 ± 0.002	0.26 ± 0.013	5	
5h	2-Naphthyl	0.67 ± 0.027	0.56 ± 0.017	0.81 ± 0.032		
5i	4-Biphenyl	2.80 ± 0.140	2.20 ± 0.088	2.76 ± 0.110		
2^b		0.05	0.15	0.02		7
3^b		0.23	0.18	0.09		
TSA		0.007	0.0004	0.0008		
SAHA		0.05	0.03	0.20	7	

^a Data represent mean values of at least three separate experiments.

^b Ragno et al. (2004).

2.5.7. Granulocytic differentiation on U937 cells

Granulocytic differentiation was carried out as previously described (Altucci et al., 2001). Briefly, U937 cells were harvested and resuspended in 10 μl phycoerythrin-conjugated CD11c (CD11c-PE). Control samples were incubated with 10 μl PE conjugated mouse IgG1, incubated for 30 min at 4 °C in the dark, washed in PBS and resuspended in 500 μl PBS containing PI (0.25 μg/mL). Samples were analysed by FACS with Cell Quest technology (Becton Dickinson). PI positive cells have been excluded from the analysis.

2.5.8. Determination of p21^{WAF1/CIP1} induction in U937 cells

100 μg of total protein extracts were separated on a 15% polyacrylamide gel and blotted as previously described (Altucci et al., 2001; Nebbioso et al., 2005). Western blots were shown for p21 (Transduction Laboratories, dilution 1:500) and total ERKs (Santa Cruz) were used to normalise for equal loading.

2.5.9. Histone H3 and α-tubulin acetylation in U937 cells

For determination of α-tubulin acetylation, 25 μg of total protein extracts were separated on a 10% polyacrylamide gel with subsequent blotting. Western blots were prepared for acetylated α-tubulin (Sigma, dilution 1:500), and total ERKs (Santa Cruz, dilution 1:1000) were used to normalise for equal loading. For quantification of histone H3 acetylation, 5 μg of histone extracts were separated on a 15% polyacrylamide gel with subsequent blotting. Western blots were prepared for acetylated histone H3 (Upstate), and total ERKs (Santa Cruz) were used to normalise for equal loading.

3. Results

3.1. Enzyme inhibitory activities, structure–activity relationship and binding mode analysis

3.1.1. Maize HD2, HD1-B, and HD1-A inhibitory activities

The novel *iso*-APHA derivatives **4** and **5** were evaluated for their ability to inhibit the three maize enzymes HD2 (a plant specific form) (Lusser et al., 1997), HD1-B (class I HDAC homologue) (Kolle et al., 1999; Lechner et al., 2000) and HD1-A (class II HDAC homologue) (Brosch et al., 1992, 1996a), SAHA (Richon et al., 1998), TSA (Yoshida

et al., 1990), and compounds **2** and **3** (Ragno et al., 2004) were used as reference drugs. The results, expressed as 50% inhibitory concentration (IC₅₀) values, are reported in Table 3. The resulting fold selectivity values (for class I HDACs: IC_{50-HD1-A}/IC_{50-HD1-B} ratio; for class II HDACs: IC_{50-HD1-B}/IC_{50-HD1-A}) ratio) were also calculated.

First, the novel derivatives **4a–i** and **5a–i** were routinely tested against maize HD2. In this assay the insertion of the same substituent had different effects on the two series. While in the 2,4-disubstituted pyrroles **4a–c** the insertion of a methyl group at the benzoyl moiety weakly decreased the HD2 inhibiting activity according to the order *para* > *meta* > *ortho* in respect to the unsubstituted analogue **2**, in the 2,5-disubstituted pyrroles **5a–c** the introduction of the same group had no significant influence on the inhibiting activity. The chlorine atom, however in **4d–f** resulted in a general drop (about three to four times) of anti-HD2 activity, in **5d–f** resulted in a compound (**5f**) as potent as **3** when introduced at the *para* position, and either a less (1.4-fold) or a more (2.4-fold) active derivative (**5d** or **5e**, respectively) when it was inserted at the *ortho* or the *meta* position, respectively. The replacement of the benzene ring of **2** and **3** with the bulkier 1-naphthyl group led to **4g** and **5g**, that were 3.8- and 2-fold more potent than the corresponding benzoyl analogues, respectively. Compounds **4h** and **4i**, bearing a 2-naphthyl and 4-biphenyl moieties, conserved the same activity as **2**, whereas in the **5** series the corresponding **5h** and **5i** were both less active than the reference compound **3**.

In the anti-HD1-B assay, the insertion of a methyl group at the *para* position of the benzoyl moiety (**4c**), as well as the replacement of the benzoyl group with the bulkier 1- and 2-naphthyl or the 4-biphenyl group (**4g–i**) led to an increase of activity with respect to **2**, whereas against HD1-A only a methyl group at the *ortho* (**4a**) or *meta* (**4b**) position of the benzoyl portion was tolerated, all the other chemical manipulation yielding less potent compounds than **2**. In the **5** series, the change of the benzoyl moiety with the 1-naphthyl one (**5g**) led to an increase of the inhibiting potency against HD1-B, while against HD1-A the 3-Me, 4-Me, and 3-Cl derivatives (**5b**, **5c**, and **5e**) were as active as the unsubstituted **3**, with all remaining compounds being less potent.

Regarding the selectivity, only a ratio >3 between the HD1-B and HD1-A IC₅₀ values has been considered. Thus, **4a** and **4b** showed

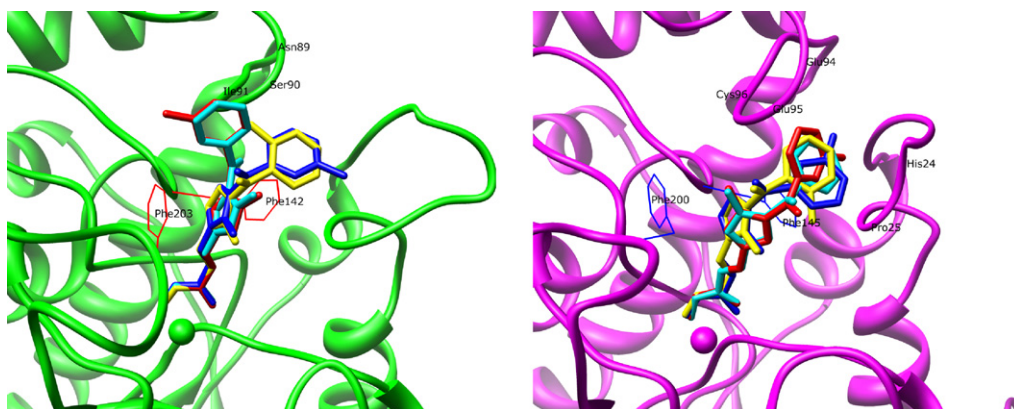


Fig. 2. Compounds **2** (cyan), **4b** (red), **5a** (yellow), and **5b** (blue) as docked on maize HD1-A (left) and maize HD1-B (right) proteins. (For interpretation of the references to colour in this figure legend, the reader is referred to the web version of the article.)

higher class II-selectivity than their reference **2**, and among the compounds of the **5** series, **5e** was 10-fold selective for the class II enzyme. As regards to class I selectivity, it is noteworthy that in both the pyrrole series the 1-naphthoyl substituted compounds **4g** and **5g** showed seven- and fivefold higher inhibiting activities against the class I enzyme HD1-B, than against HD1-A (class II), respectively.

3.1.2. Molecular modelling and docking studies

Homology models for the HD1-A and HD1-B sequences were derived by using the CPHmodels 2.0 Server using structural data from the HDAC8/TSA complex (PDB code: 1T64) (Somoza et al., 2004). Subsequently, a molecular dynamics (MD) protocol (see Section 2) was employed to refine the HD1-A and HD1-B models complexed with the reference drug SAHA. The AutoDock 3.0.5

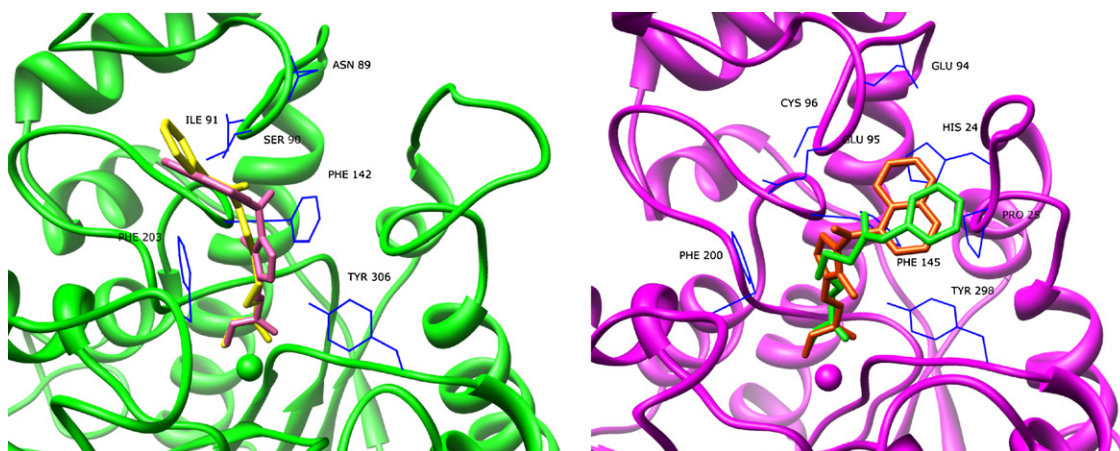


Fig. 3. Compound **4g** docked into HD1-A (left, in pink) and HD1-B (right, in orange). SAHA bound conformation is also displayed (yellow in left side and green in right side) for comparison purposes. (For interpretation of the references to colour in this figure legend, the reader is referred to the web version of the article.)

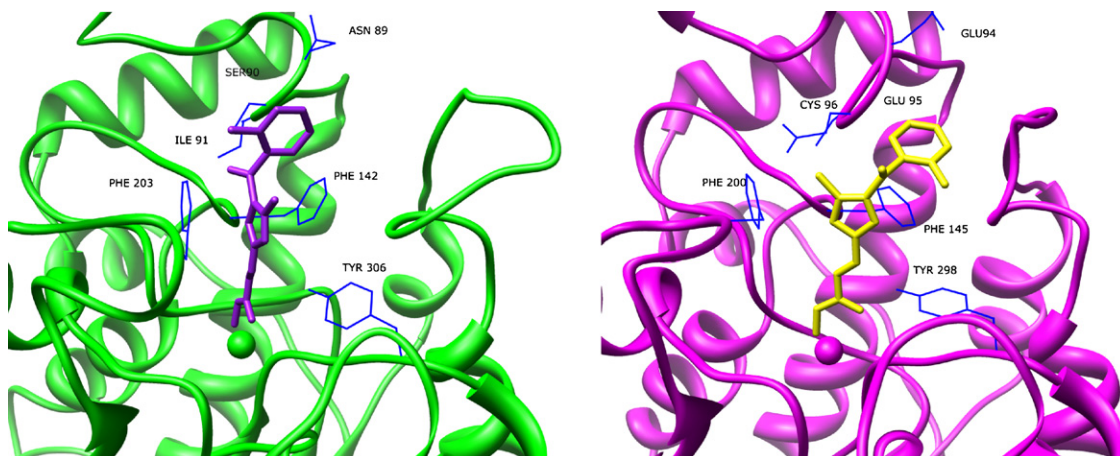


Fig. 4. Compound **4a** docked into HD1-A (left) and HD1-B (right).

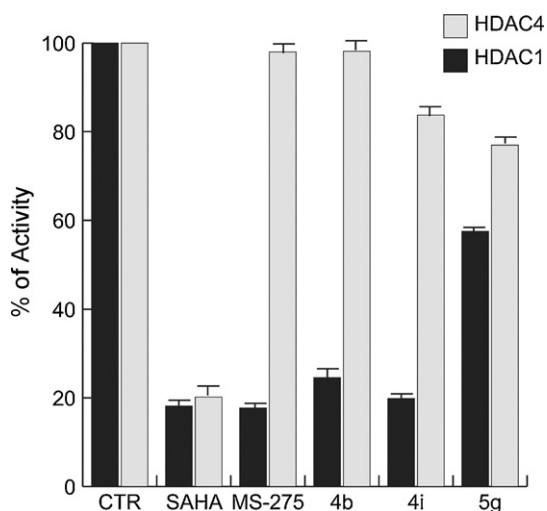


Fig. 5. HDAC1 and HDAC4 IP inhibitory activities of compounds **4b**, **4i**, and **5g** tested at 5 μ M.

and 4.0.1 programs (Goodsell et al., 1996; Morris et al., 1996, 1998) were used to explore the binding mode of all derivatives. The docking studies were conducted twofold, first considering the receptor completely rigid, and then letting Tyr306 (HD1-A) or Tyr298 (HD1-B) side-chain to be flexible. The choice to allow these residues to move rely to the structural information available. In fact, the Tyr306/Tyr298 hydroxyl groups have been reported to make an hydrogen bond with the hydroxamate carbonyl group of either TSA or SAHA (Finnin et al., 1999; Nielsen et al., 2005). As a general observation, the lowest energy conformation of the most populated clusters obtained from the docking runs showed that all the molecules into either HD1-A or HD1-B proved to be able to chelate the zinc ion in a quasi optimal geometry (average distances: CO...Zn=2.37 Å, OH...Zn=1.87 Å). In particular, a deeper inspection revealed that in HD1-A, the 2,4-disubstituted (**4a–i**) and 2,5-disubstituted (**5a–i**) pyrroles presented the *N*-methylpyrrole ring stacking between Phe142 and Phe203 phenyl rings, with the methyl moiety turned in the same direction (Fig. 2). Regarding the aroyl moieties, the two series displayed a switched and shifted position of the aroyl groups. Derivatives **4** have a general binding conformation in which the aroyl group is oriented towards the Asn89-Ser90-Ile91 residues, establishing positive hydrophobic interactions, while for the **5** series was not possible to record any important interaction, being the aroyl moieties mainly turned inward the entrance of the

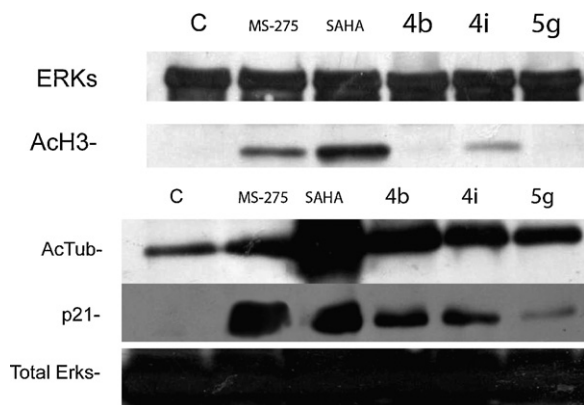


Fig. 6. Acetylation assays on histone H3 and α -tubulin, and p21 induction by **4b**, **4i**, and **5g** on U937 cells. Total ERKs were used to normalize for equal loading.

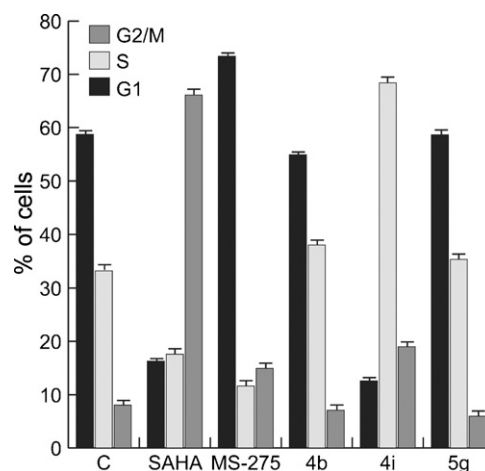


Fig. 7. Effects of the iso-APHAs **4b**, **4i**, and **5g** on the cell cycle in the human leukemia U937 cell line, tested at 5 μ M for 30 h.

channel of the HD1-A enzyme. This binding mode profile is in good agreement with the experimental biological observation and might explain the lower HD1-A inhibitory activity of the 2,5-disubstituted pyrroles **5**.

On the other hand, the docked conformation of the two series **4** and **5** into HD1-B presented the aroyl moieties docked in the same receptor space, and again it is in agreement with the enzyme-based assay where the two series **4** and **5** showed similar anti-HD1-B activities (Fig. 2). As the main structural differences between HD1-A and HD1-B were located at the Asn89-Ser90-Ile91 (HD1-A) and Glu94-Glu95-Cys96 (HD1-B) residues, this could be one of the structural parameters to explain the observed selectivity of some compounds against one of the two enzymes. In an attempt to rationalize the selectivity issue the two glutamic residues of HD1-B (Glu94-Glu95) create a mainly negatively charged molec-

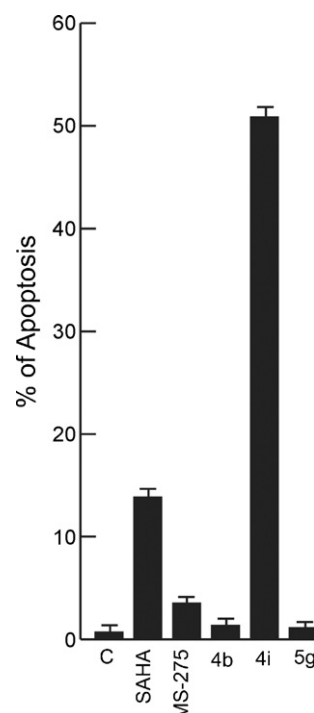


Fig. 8. Apoptosis on human leukemia U937 cells induced by the iso-APHAs **4b**, **4i**, and **5g**, tested at 5 μ M for 30 h.

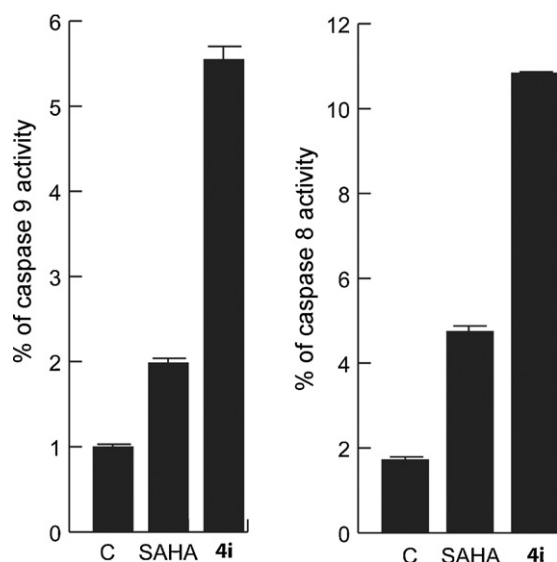


Fig. 9. Caspase 8 and 9 activity assays performed with **4i** and SAHA at 5 μ M for 18 h in the U937 cells.

ular environment (different electrostatic potentials and surfaces) at the HD1-B channel entrance, whereas in HD1-A although there are hydrophilic residues (Asn89-Ser90), the surrounding space is mainly neutral (Fig. S1 in Supplementary material). A further structural difference can be found between the HD1-A/Tyr204 and the corresponding HD1-B/Tyr199: the side-chains of these two tyrosines occupy different spatial areas as displayed in Fig. S1. The above listed structural variances could determine the different SAHA binding modes that have been experimentally observed in the bacterial class I HDAC homologue HDLP (Finnin et al., 1999) (the first HDAC homologue that have been described in complex with SAHA and TSA), and in the recently described class II bacterial HDAC (HDAH) (Nielsen et al., 2005). Such different SAHA binding conformations were also recorded by the docking experiments of SAHA in the two modelled maize enzymes. The HD1-A/SAHA conformation displayed the phenyl portion in proximity of the Ser90 and Tyr204 residues (not shown), making some unfavourable steric interactions between the hydrophobic SAHA phenyl ring and the Ser90/Tyr204 hydroxyl groups, while in HD1-B the same moiety approached to the His24 and Pro25 (Fig. S1) making some levels of positive steric interactions. The two SAHA HD1-A and HD1-B bound conformations are likely related to the different enzyme structural environments above highlighted, and the different interaction profile is in agreement with the fact that SAHA is a slightly class I selective HDACi as reported in Table 3.

Although the newly synthesized compounds are not highly selective against either class I or class II HDAC homologues, a few of them showed some level of selectivity index for HD1-A or HD1-B. Interestingly, the docking experiments on all the compounds belonging to **4** and **5** series led to binding conformations overlapping to those of SAHA (not shown). To focus on the class selectivity

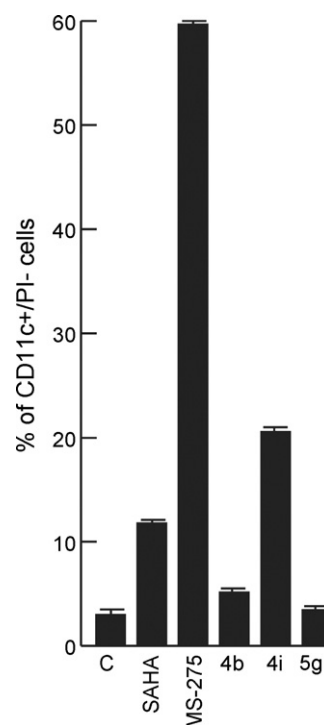


Fig. 11. Granulocytic differentiation on human leukemia U937 cells exerted by the iso-APHAs **4b**, **4i**, and **5g** tested at 5 μ M for 30 h, as determined by the CD11c expression levels.

topic, we analysed the binding modes of **4a** and **4g**, two class II- and class I-selective HDACi, respectively. Compound **4g** presented the HD1-A and HD1-B docked conformations overlapped to the respective SAHA structures (Fig. 3). Similarly to SAHA, the HD1-B docked **4g** conformation displayed the aromatic naphthyl portion close to the His24 and Pro25 residues, in agreement with the sevenfold higher selectivity for this enzyme. A general inspection of the molecules with bulky aromatic moieties revealed that they prefer binding conformations in which the cap portion interacts with the His24 and Pro25 HD1-B residues, while on HD1-A they resulted turned towards to HD1-A Asn89-Ser90-Ile91 thus making less hydrophobic interactions. The result is a few HD1-B selectivity.

Compound **4a** places the *ortho*-methylphenyl moiety close to the HD1-A Asn89-Ser90-Ile91 backbone with positive contribution interactions, while in the HD1-B enzyme the aromatic portion did not show any interactions thus leading to class II selectivity (Fig. 4).

As mentioned above, recently the structure of a class II bacterial HDAC homologue (HDAH) have been reported and made publicly available. To assess our docking experiments, in parallel we applied the docking procedure also using the experimental structure of either HDLP (Finnin et al., 1999) (bacterial class I homologue) or HDAH (Nielsen et al., 2005). Analyses of the **4** and **5** docked conformations in the experimental classes I and II HDACs revealed comparable results.

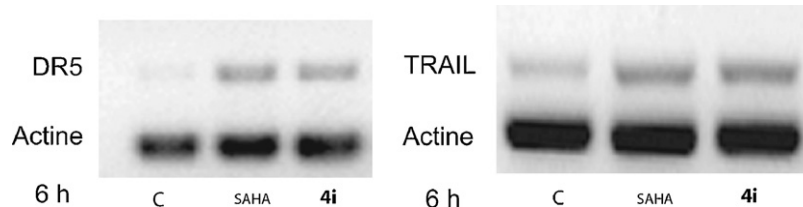


Fig. 10. TRAIL and DR5 induction by **4i** and SAHA at 5 μ M after 6 h in the U937 cells.

3.1.3. *In vivo* human HDAC1 and HDAC4 inhibitory activities

On the selected compounds **4b**, **4i**, and **5g** the inhibitory activity against human HDAC1 and HDAC4 was determined. HDAC1 and HDAC4 immunoprecipitates (IPs) were obtained from human leukemia U937 and breast cancer ZR-75.1 cell lysates, respectively, with the appropriate antibodies [anti-HDAC1 (Abcam) in U937, and anti-HDAC4 (Sigma) in ZR-75.1 cells]. The *iso*-APHA derivatives as well as SAHA and MS-275 (taken as reference drugs) were used at 5 μ M. Fig. 5 shows the inhibitory effects of the tested compounds against the HDAC1 and HDAC4 IPs. Against human HDAC1, the two 2,4-disubstituted pyrrole derivatives **4b** and **4i** showed high inhibitory activities (% inhibition: **4b**, 75.5%; **4i**, 80.2%) fully comparable to that of the reference drugs (% inhibition: MS-275, 82.3%; SAHA, 81.9%), whereas the 2,5-disubstituted **5g** was less effective (% inhibition: 42.5%). In the anti-HDAC4 (a class IIa enzyme) assay, **4b** was totally inactive at the tested concentration (5 μ M), and **4i** and **5g** displayed only weak inhibitory activity (**4i**, 16.2%; **5g**, 23.1%) when compared to SAHA (79.8% inhibition).

3.2. H3 histones and α -tubulin acetylation assays. Induction of p21^{WAF1}

Functional tests on the selected **4b**, **4i**, and **5g** were performed in addition to the enzymatic assays. To this aim, the capacity to induce acetylation was tested using H3 histones and α -tubulin (a non-histone substrate) as substrates of acetylation. Moreover, the capability of induction of the cyclin dependent kinase inhibitor p21^{WAF1/CIP1} for the tested compounds was assessed. H3 histone acetylation assay was performed by treating the U937 cells with the *iso*-APHAs or with SAHA and MS-275 (all at 5 μ M) for 24 h. Then, the total protein extracts were separated and blotted, and Western blots have been performed for acetylated histone H3. To determine the α -tubulin acetylation extent and p21 induction, the extracts were treated with the pyrroles and SAHA (all at 5 μ M), and then separated and blotted after 24 h. Total ERKs were used to normalize for equal loading (Fig. 6).

On H3 histones, among the pyrrole compounds only **4i** showed an acetylating effect. With α -tubulin as a substrate, all the three tested compounds displayed high acetylating activity, according to the order **4b** > **4i** > **5g**. As regards to p21 induction, **4b** and **4i** highly induced p21 expression, whereas **5g** displayed only weak activity.

3.3. Effects on human leukemia U937 cells: cell cycle, apoptosis induction, and granulocytic differentiation

Compounds **4b**, **4i**, and **5g** were then tested in the human leukemia U937 cell line to evaluate their effects on cell cycle, apoptosis induction, and granulocytic differentiation. SAHA and MS-275 were also tested for comparison purpose. All the compounds were tested at 5 μ M and after 30 h of incubation the observed effects were recorded. In the U937 cells, **4b** and **5g** did not alter the cell cycle phases, whereas **4i** and SAHA showed an arrest in the S (**4i**) or G2 (SAHA) phase, and MS-275 displayed a block in the G1 phase at the tested conditions (Fig. 7).

The apoptosis induction in U937 cells was evaluated through Annexin V/propidium iodide (PI) double staining by FACS analysis, and was checked after 30 h of treatment of the cells with 5 μ M *iso*-APHAs, SAHA, and MS-275. In these conditions, **4b** and **5g** failed in inducing apoptosis, whereas **4i** showed 51% of apoptosis thus being also more efficient than SAHA (14%) (Fig. 8).

To investigate the apoptotic action of compound **4i** and SAHA at the molecular level, we performed a caspase assay for caspase 8 and 9, taken as readout of the extrinsic and intrinsic pathway of apoptosis respectively in the U937 cells. As clearly shown in Fig. 9, compound **4i** seems to activate both caspases more efficiently

than SAHA, being more active on caspase 8 activation. Taking into account that HDACi have been reported to act in leukemias via the TNF-related apoptosis-inducing ligand (TRAIL) pathway activation (Nebbioso et al., 2005; Manzo et al., 2008; Altucci et al., 2005), we investigated if compound **4i** was able to induce TRAIL or its cognate apoptotic receptor DR5. As shown in Fig. 10, both TRAIL and DR5 are induced upon 6 h of **4i** treatment in the U937 cells, thus confirming an activation of this pathway.

The CD11c expression level was used as a marker for the evaluation of granulocytic differentiation in U937 cells. After 30 h of stimulation, among the tested *iso*-APHAs only **4i** showed a differentiation activity (21% CD11c positive/propidium iodide (PI) negative cells), superior to that of SAHA (14%) but much lower than MS-275 level (60%) (Fig. 11).

4. Discussion

Starting from the two APHAs isomers, the 3-(2-benzoyl-1-methyl-1H-pyrrol-4-yl)-N-hydroxy-2-propenamide **2** and the 3-(2-benzoyl-1-methyl-1H-pyrrol-5-yl)-N-hydroxy-2-propenamide **3**, some chemical modifications at their aryl moieties were performed. In particular, methyl groups or chlorine atoms were introduced at the three positions of the **2** and **3** C2-benzoyl portion, or the same moiety was replaced by 1- and 2-naphthyl and 4-biphenyl groups. When the obtained *iso*-APHAs **4a–i** and **5a–i** were tested against the maize deacetylases HD2, HD1-B (class I HDAC homologue) and HD1-A (class II HDAC homologue), inhibitory activities in the submicromolar to nanomolar range were registered. Some of the tested compounds shared a little class I selectivity (**4g**, **4i**, and **5g**), while others (**4a**, **4b**, **4e**, **5c**, and **5e**) preferentially inhibited the class II enzyme.

Molecular modelling studies were performed to gather insight on the observed inhibition differences. Besides maize enzymes, the docking studies were conducted on two bacterial enzymes, HDAH (1ZZ1) (Nielsen et al., 2005) and HDLP (1C3S) (Finnin et al., 1999), homologues of mammalian class II and class I HDACs, respectively. The analyses of the docked **4** and **5** derivatives indicated that different activities were likely to reside on the aromatic portion (cap group). Smaller hydrophobic cap groups (compare **4a** and **4b** with **2**) may improve class II HDAC selectivity through the interaction with the HD1-A Asn89-Ser90-Ile91 residues, while the bulkier aromatic substituents increase class I HDAC selectivity (compare **4g**, **4i**, and **5g** with both **2** and **3**).

Selected compounds (**4b**, **4i**, and **5g**) were tested against human HDAC1 and HDAC4 IPs obtained from human leukaemia U937 and breast cancer ZR-75.1 cell lysates, respectively. At 5 μ M, compounds **4b** and **4i** showed HDAC1 inhibition similar to that of SAHA and MS-275, used as reference drugs, whereas **5g** was less effective. The inhibitory effects of the tested *iso*-APHAs against HDAC4 were much less noticeable, **4b** being totally inactive and **4i** and **5g** showing just a marginal inhibition. In functional assays (histone H3 and α -tubulin acetylation, to test the class I and class IIb inhibitory action, respectively), at 5 μ M **4i** gave a weak signal for acetyl-H3, whereas the all three tested compounds were able to increase the tubulin acetylation levels, with **4b** which was the most potent. When tested to study their capability to induce the CDK inhibitor p21, **4b** and **4i** gave appreciable signals whereas **5g** was much less active.

Taking into account the whole enzyme data and the functional test results, the described *iso*-APHAs showed a behaviour of class I/IIb HDACi. In particular, **4b** seems to be preferentially a class IIb inhibitor (highly active against HD1-A and powerful in increasing the acetyl-tubulin level), and **4i** seems to be a class I (high anti-HD1-B and -HDAC1 activity, histone H3 increased acetylation, p21 induction) and, to a lesser extent, class IIb inhibitor.

Such inhibitor profiles were confirmed by the effects of **4b**, **4i**, and **5g** by determining the cell cycle, the apoptosis induction, and granulocytic differentiation in U937 cells. At 5 μ M, after 30 h of treatment only **4i** among the tested iso-APHAs showed altered cell cycle (S phase arrest), also displaying high (51%) apoptosis induction and significant (21%) differentiation activity. In comparison with SAHA (pan-HDACi) and MS-275 (class I HDACi), at the tested concentration **4i** was 3.6- and 17-fold more potent than SAHA and MS-275, respectively, in inducing apoptosis, and 2-fold more efficient than SAHA and 3-fold less active than MS-275 to induce granulocytic differentiation. The high apoptotic effect of **4i** could be explained, at least in part, through caspases 8 and 9 activation. The development of compounds such as **4i** with a peculiar profile of inhibition towards the different classes of HDACs could be useful to dissect the biological functions of these enzymes and may represent, for example in association with other pro-apoptotic drugs, a valuable way for cancer therapy.

Acknowledgements

This work was partially supported by grants from AIRC 2007 (AM), PRIN 2006 (AM and LA), European Union (HEALTH-F4-2007-200767) (LA), FIRB RBIP067F9E and RETI FIRB RBPR05NWWC.006 (AM). FM is a PhD student of the Italian-French University. SS is a fellow of Istituto Pasteur, Fondazione Cenci-Bolognetti (Rome).

Appendix A. Supplementary data

Supplementary data associated with this article can be found, in the online version, at doi:10.1016/j.biocel.2008.09.002.

References

- Altucci L, Rossin A, Raffelsberger W, Reitmair A, Chomienne C, Gronemeyer H. Retinoic acid-induced apoptosis in leukemia cells is mediated by paracrine action of tumor-selective death ligand TRAIL. *Nat Med* 2001;7:680–6.
- Altucci L, Clarke N, Nebbioso A, Scognamiglio A, Gronemeyer H. Acute myeloid leukemia: therapeutic impact of epigenetic drugs. *Int J Biochem Cell Biol* 2005;37:1752–62.
- Artico M, Corelli F, Massa S, Stefancich G. Nonsteroidal antiinflammatory agents. 1. A novel synthesis of 1-methyl-5-p-tolylpyrrole-2-acetic acid (Tolmetin). *J Heterocycl Chem* 1982;19:1493–5.
- Bolden JE, Peart MJ, Johnstone RW. Anticancer activities of histone deacetylase inhibitors. *Nat Rev Drug Discov* 2006;5:769–84.
- Brosch G, Georgieva EI, Lopez-Rodas G, Lindner H, Loidl P. Specificity of *Zea mays* histone deacetylase is regulated by phosphorylation. *J Biol Chem* 1992;267:20561–4.
- Brosch G, Goralik-Schramel M, Loidl P. Purification of histone deacetylase HD1-A of germinating maize embryos. *FEBS Lett* 1996a;393:287–91.
- Brosch G, Lusser A, Goralik-Schramel M, Loidl P. Purification and characterization of a high molecular weight histone deacetylase complex (HD2) of maize embryos. *Biochemistry (Mosc)* 1996b;35:15907–14.
- Budillon A, Di Gennaro E, Bruzzese F, Rocco M, Manzo G, Caraglia M. Histone deacetylase inhibitors: a new wave of molecular targeted anticancer agents. *Recent Patients Anticancer Drug Discov* 2007;2:119–34.
- Butler KV, Kozikowski AP. Chemical origins of isoform selectivity in histone deacetylase inhibitors. *Curr Pharm Des* 2008;14:505–28.
- Carson JR, Codd EE, Pitis PM. Preparation of (aroyl)pyrrolyl heteroaryl methanones and methanols as central nervous system agents. *PCT/WO/2003/057219*; 2003a [December 10, 2002].
- Carson JR, Codd EE, Pitis PM. Preparation of (aroyl)pyrrolyl heteroaryl methanones and methanols as central nervous system agents. *PCT/WO/2003/057147*; 2003b [December 23, 2002].
- Carson JR, Davis NM. Acid-mediated rearrangement of acylpyrroles. *J Org Chem* 1981;46:839–43.
- Carson JR, Pitis PM. Preparation of aroyl aminoacyl pyrroles as CNS agents. *PCT/WO/2002002521*; 2002 [June 29, 2001].
- Carson JR, Pitis PM, Rogers KE. Preparation of aminoacyl(aroyl)pyrroles for treatment of neuropathic pain. *PCT/WO/2000048584*; 2000 [February 17, 2000].
- Case DA, Cheatham III TE, Darden T, Gohlke H, Luo R, Merz Jr KM, et al. The Amber biomolecular simulation programs. *J Comput Chem* 2005;26:1668–88.
- Cheung WL, Briggs SD, Allis CD. Acetylation and chromosomal functions. *Curr Opin Cell Biol* 2000;12:326–33.
- Condorelli F, Gnemmi I, Vallario A, Genazzani AA, Canonico PL. Inhibitors of histone deacetylase (HDAC) restore the p53 pathway in neuroblastoma cells. *Br J Pharmacol* 2008;153:657–68.
- Corelli F, Massa S, Stefancich G, Mai A, Artico M, Panico S, et al. Antibacterial and antifungal compounds. VIII. Synthesis and antifungal activity of pyrrol derivatives similar to trichostatin A. *Farmacology [Sci]* 1987;42:893–903.
- Finnin MS, Donigian JR, Cohen A, Richon VM, Rifkind RA, Marks PA, et al. Structures of a histone deacetylase homologue bound to the TSA and SAHA inhibitors. *Nature* 1999;401:188–93.
- Glozak MA, Sengupta N, Zhang X, Seto E. Acetylation and deacetylation of non-histone proteins. *Gene* 2005;363:15–23.
- Goodsell DS, Morris GM, Olson AJ. Automated docking of flexible ligands: applications of AutoDock. *J Mol Recogn* 1996;9:1–5.
- Grant S, Easley C, Kirkpatrick P. Vorinostat. *Nat Rev Drug Discov* 2007;6:21–2.
- Grozinger CM, Schreiber SL. Deacetylase enzymes: biological functions and the use of small-molecule inhibitors. *Chem Biol* 2002;9:3–16.
- Itoh Y, Suzuki T, Miyata N. Isoform-selective histone deacetylase inhibitors. *Curr Pharm Des* 2008;14:529–44.
- Jain AN. Surflex-Dock 2.1: robust performance from ligand energetic modeling, ring flexibility, and knowledge-based search. *J Comput Aided Mol Des* 2007;21:281–306.
- Jones P, Steinkuhler C. From natural products to small molecule ketone histone deacetylase inhibitors: development of new class specific agents. *Curr Pharm Des FIELD (Full Journal Title: Current Pharmaceutical Design)* 2008;14:545–61.
- Khan N, Jeffers M, Kumar S, Hackett C, Boldog F, Khramtsov N, et al. Determination of the class and isoform selectivity of small-molecule histone deacetylase inhibitors. *Biochem J* 2008;409:581–9.
- Kolle D, Brosch G, Lechner T, Lusser A, Loidl P. Biochemical methods for analysis of histone deacetylases. *Methods* 1998;15:323–31.
- Kolle D, Brosch G, Lechner T, Pipal A, Helliger W, Taplick J, et al. Different types of maize histone deacetylases are distinguished by a highly complex substrate and site specificity. *Biochemistry (Mosc)* 1999;38:6769–73.
- Kouzarides T. Histone acetylases and deacetylases in cell proliferation. *Curr Opin Genet Dev* 1999;9:40–8.
- Krause S, Willighagen E, Steinbeck C. JChemPaint—using the collaborative forces of the internet to develop a free editor for 2D chemical structures. *Molecules* 2000;5:93–8.
- Lechner T, Lusser A, Brosch G, Eberharter A, Goralik-Schramel M, Loidl P. A comparative study of histone deacetylases of plant, fungal and vertebrate cells. *Biochim Biophys Acta* 1996;1296:181–8.
- Lechner T, Lusser A, Pipal A, Brosch G, Loidl A, Goralik-Schramel M, et al. RPD3-type histone deacetylases in maize embryos. *Biochemistry (Mosc)* 2000;39:1683–92.
- Lee SJ, Seko T, Frierson MR, Sircar JC, Cao CX. Preparation of 2-(pyrrol-2-yl)acetic acids as 5 α -reductase inhibitors. *PCT/WO/9610013*; 1996 [September 27, 1995].
- Lusser A, Brosch G, Loidl A, Haas H, Loidl P. Identification of maize histone deacetylase HD2 as an acidic nucleolar phosphoprotein. *Science* 1997;277:88–91.
- Mai A, Massa S, Cerbara I, Valente S, Ragno R, Bottoni P, et al. 3-(4-Aroyl-1-methyl-1H-2-pyrrolyl)-N-hydroxy-2-propenamides as a new class of synthetic histone deacetylase inhibitors. 2. Effect of pyrrole-C2 and/or -C4 substitutions on biological activity. *J Med Chem* 2004;47:1098–109.
- Mai A, Massa S, Pezzi R, Rotili D, Loidl P, Brosch G. Discovery of (aryloxypropenyl)pyrrolyl hydroxyamides as selective inhibitors of class IIa histone deacetylase homologue HD1-A. *J Med Chem* 2003;46:4826–9.
- Mai A, Massa S, Ragno R, Esposito M, Sbardella G, Nocca G, et al. Binding mode analysis of 3-(4-benzoyl-1-methyl-1H-2-pyrrolyl)-N-hydroxy-2-propenamide: a new synthetic histone deacetylase inhibitor inducing histone hyperacetylation, growth inhibition, and terminal cell differentiation. *J Med Chem* 2002;45:1778–84.
- Mai A, Massa S, Valente S, Simeoni S, Ragno R, Bottoni P, et al. Aroyl-pyrrolyl hydroxyamides: influence of pyrrole C4-phenylacetyl substitution on histone deacetylase inhibition. *ChemMedChem* 2006;1:225–37.
- Mai A, Valente S, Rotili D, Massa S, Botta G, Brosch G, et al. Novel pyrrole-containing histone deacetylase inhibitors endowed with cytodifferentiation activity. *Int J Biochem Cell Biol* 2007;39:1510–22.
- Manzo F, Nebbioso A, Miceli M, Conte M, De Bellis F, Carafa V, et al. TNF-related apoptosis-inducing ligand: signalling of a 'smart' molecule. *Int J Biochem Cell Biol* 2008;012, doi:10.1016/j.biocel.2007.12.012.
- Marks PA, Breslow R. Dimethyl sulfoxide to vorinostat: development of this histone deacetylase inhibitor as an anticancer drug. *Nat Biotechnol* 2007;25:84–90.
- Marumo S, Aoyagi K, Hamamura H, Nakayama A, Sano H. Preparation of 2-acylpyrrole derivatives, 2-furoyl, and 2-thenoyl derivatives as agricultural or horticultural fungicides. *PCT/WO/2002085852*; 2002 [April 17, 2002].
- Massa S, Mai A, Sbardella G, Esposito M, Ragno R, Loidl P, et al. 3-(4-Aroyl-1H-pyrrol-2-yl)-N-hydroxy-2-propenamides, a new class of synthetic histone deacetylase inhibitors. *J Med Chem* 2001;44:2069–72.
- Minucci S, Pelicci PG. Histone deacetylase inhibitors and the promise of epigenetic (and more) treatments for cancer. *Nat Rev Cancer* 2006;6:38–51.
- Morris GM, Goodsell DS, Huey R, Olson AJ. Distributed automated docking of flexible ligands to proteins: parallel applications of AutoDock 2.4. *J Comput Aided Mol Des* 1996;10:293–304.
- Morris GM, Goodsell DS, Halliday RS, Huey R, Hart WE, Belew RK, et al. Automated docking using a Lamarckian genetic algorithm and empirical binding free energy function. *J Comput Chem* 1998;19:1639–62.

- Nebbioso A, Clarke N, Voltz E, Germain E, Ambrosino C, Bontempo P, et al. Tumor-selective action of HDAC inhibitors involves TRAIL induction in acute myeloid leukemia cells. *Nat Med* 2005;11:77–84.
- Nielsen TK, Hildmann C, Dickmanns A, Schwienhorst A, Ficner R. Crystal structure of a bacterial class 2 histone deacetylase homologue. *J Mol Biol* 2005;354:107–20.
- Pettersen EF, Goddard TD, Huang CC, Couch GS, Greenblatt DM, Meng EC, et al. UCSF chimera—a visualization system for exploratory research and analysis. *J Comput Chem* 2004;25:1605–12.
- Ragno R, Mai A, Massa S, Cerbara I, Valente S, Bottoni P, et al. 3-(4-Aroyl-1-methyl-1H-pyrrol-2-yl)-N-hydroxy-2-propenamides as a new class of synthetic histone deacetylase inhibitors 3. Discovery of novel lead compounds through structure-based drug design and docking studies. *J Med Chem* 2004;47:1351–9.
- Ragno R, Simeoni S, Rotili D, Caroli A, Botta G, Brosch G, et al. Class II-selective histone deacetylase inhibitors. Alignment-independent GRIND 3-D QSAR, homology and docking studies. *Eur J Med Chem FIELD (Full Journal Title: European Journal of Medicinal Chemistry)* 2008;43:621–32.
- Ragno R, Simeoni S, Valente S, Massa S, Mai A. 3-D QSAR studies on histone deacetylase inhibitors. A GOLPE/GRID approach on different series of compounds. *J Chem Inform Model* 2006;46:1420–30.
- Richon VM, Emiliani S, Verdin E, Webb Y, Breslow R, Rifkind RA, et al. A class of hybrid polar inducers of transformed cell differentiation inhibits histone deacetylases. *Proc Natl Acad Sci USA* 1998;95:3003–7.
- Somoza JR, Skene RJ, Katz BA, Mol C, Ho JD, Jennings AJ, et al. Structural snapshots of human HDAC8 provide insights into the class I histone deacetylases. *Structure* 2004;12:1325–34.
- Steinbeck C, Han Y, Kuhn S, Horlacher O, Luttmann E, Willighagen E. The chemistry development kit (CDK): an open-source Java library for Chemo- and bioinformatics. *J Chem Inform Comput Sci* 2003;43:493–500.
- Steinbeck C, Hoppe C, Kuhn S, Floris M, Guha R, Willighagen EL. Recent developments of the chemistry development kit (CDK)—an open-source java library for chemo- and bioinformatics. *Curr Pharm Des* 2006;12:2111–20.
- Strahl BD, Allis CD. The language of covalent histone modifications. *Nature* 2000;403:41–5.
- Vigushin DM, Coombes RC. Histone deacetylase inhibitors in cancer treatment. *Anti-cancer Drugs* 2002;13:1–13.
- Wolffe AP, Guschin D. Review: chromatin structural features and targets that regulate transcription. *J Struct Biol* 2000;129:102–22.
- Wu J, Grunstein M. 25 years after the nucleosome model: chromatin modifications. *Trends Biochem Sci* 2000;25:619–23.
- Yoshida M, Kijima M, Akita M, Beppu T. Potent and specific inhibition of mammalian histone deacetylase both in vivo and in vitro by trichostatin A. *J Biol Chem* 1990;265:17174–9.